

MRS **Bulletin**

September 2013 Vol. 38 No. 9
www.mrs.org/bulletin



MATERIALS RESEARCH SOCIETY
Advancing materials. Improving the quality of life.

Quantum dot light-emitting devices



ALSO IN THIS ISSUE

Climbing the ladder of density
functional approximations



Spectroscopic insights into the performance of quantum dot light-emitting diodes

Wan Ki Bae, Sergio Brovelli, and Victor I. Klimov

Lighting consumes almost one-fifth of all electricity generated today. In principle, with more efficient light sources replacing incandescent lamps, this demand can be reduced at least twofold. A dramatic improvement in lighting efficiency is possible by replacing traditional incandescent bulbs with light-emitting diodes (LEDs) in which current is directly converted into photons via the process of electroluminescence. The focus of this article is on the emerging technology of LEDs that use solution-processed semiconductor quantum dots (QDs) as light emitters. QDs are nano-sized semiconductor particles whose emission color can be tuned by simply changing their dimensions. They feature near-unity emission quantum yields and narrow emission bands, which result in excellent color purity. Here, we review spectroscopic studies of QDs that address the problem of nonradiative carrier losses in QD-LEDs and approaches for its mitigation via the appropriate design of QD emitters. An important conclusion of our studies is that the realization of high-performance LEDs might require a new generation of QDs that in addition to being efficient single-exciton emitters would also show high emission efficiency in the multicarrier regime.

Introduction: Traditional and emerging LED technologies

Beginning with the ancient myth of Prometheus, who stole fire from Mount Olympus, to third millennium technologies, the ability to master artificial light incarnates the very concept of progress and modernity. Throughout history, the impact of artificial lighting on human civilization has been so profound that it has arguably redefined our concepts of time and space, extending our productive time and allowing humankind to explore even the “darkest” corners of our world.

Our society relies so heavily on lighting that it dedicates a fifth of global electricity to it, which amounts to over 2,650 TWh of energy. In 2010, the environmental cost associated with the production of this amount of energy was equal to about two billion tons of carbon dioxide emitted in the atmosphere.¹ Unfortunately, most of this precious energy is wasted due to the inefficiency of incandescent bulbs that convert only 10% of electricity into visible light, while 90% is dissipated as heat. Fluorescent lamps are less wasteful but still have a conversion efficiency of only 20–30%. The economic advantage of overcoming these limitations, together with a growing awareness

of the harmful effects of carbon emission on global climate, has driven the tremendous effort to develop more efficient and sustainable lighting technologies.

Direct conversion of electricity into light using semiconductor-based light-emitting diodes (LEDs) is now universally accepted as the most promising approach to more efficient lighting. Solid-state lighting (SSL) sources such as LEDs demonstrate high brightness, long operational lifetime, and low energy consumption, far surpassing the performance of conventional lighting systems. The LED field is currently dominated by semiconductor quantum-well emitters (based, e.g., on InGaN/GaN) fabricated via epitaxial methods on crystalline substrates (e.g., sapphire).¹ These structures are highly efficient and bright, but their cost-to-light-output ratio (also referred to as the “cost of light”) is at least one-hundred times larger than that of incandescent light bulbs. In addition, traditional semiconductor LEDs are affected by structural defects at the substrate/semiconductor interface due to lattice mismatch and heating during operation, which limits the device area to only 1–2 mm². Furthermore, harsh conditions required for the fabrication of these structures and difficulties in post-processing

Wan Ki Bae, Chemistry Division, Los Alamos National Laboratory; wbae@lanl.gov
Sergio Brovelli, Department of Materials Science, Università degli Studi di Milano-Bicocca; sergio.brovelli@unimib.it
Victor I. Klimov, Chemistry Division, Los Alamos National Laboratory; klimov@lanl.gov
DOI: 10.1557/mrs.2013.182

complicate their use in lightweight, flexible lighting devices and displays. These drawbacks of traditional LEDs have motivated the search for new technologies, such as LEDs based on organic semiconductors (OLEDs).

OLEDs offer greatly reduced fabrication cost compared to inorganic LEDs and are easily amendable to low-temperature, large-area processing, including fabrication on flexible substrates. Synthetic organic chemistry provides essentially an unlimited number of degrees of freedom for tailoring molecular properties to achieve specific functionality, from selective charge transport to color-tunable light emission. The prospect of high-quality lighting sources based on inexpensive “plastic” materials has driven a tremendous amount of research in the area of OLEDs, which in turn has led to the realization of several OLED-based high-tech products such as flat screen televisions and mobile communication devices. Several industrial giants such as Samsung, LG, Sony, and Panasonic are working on the development of large-area white-emitting OLEDs for replacing incandescence light bulbs and fluorescent light sources.

In the most common embodiment, an OLED has a multilayer structure comprising an emissive layer (typically an organic matrix doped with molecular chromophores) sandwiched between organic hole and electron transport layers.^{2,3} The emissive chromophores are usually either conjugated fluorophores or phosphorescent metal-organic complexes.^{4,5} Conjugated fluorophores (e.g., 4-(Dicyanomethylene)-2-methyl-6-[p-(dimethylamino)styryl]-4H-pyran, coumarins and perylene derivatives)³ have been a major subject of OLED research for over two decades.^{6–8} They feature the high emission yields and short luminescence lifetimes typical of singlet emitters, which can convert the energy of singlet excitons (electron–hole pairs with total spin 0) to photons. However, their drawback is that their maximum electroluminescence (EL) internal quantum efficiency (IQE; the ratio of the number of photons emitted within a device to the number of electrons passing through the device) is limited to 25%, as 75% of excitons generated by charge injection are triplets, which are nonemissive spin 1 species. To date, external quantum efficiencies (EQEs; the ratio of the number of photons emitted from a device to the number of electrons passing through the device) of over 10% have been obtained with red^{9,10} and green¹¹ conjugated fluorophores that also demonstrate impressive device lifetimes in excess of 150,000 hours. Blue OLEDs are more difficult to realize, and so far the demonstrated EQEs from fluorescent emitters do not exceed 5–6%, and the longest lifetimes are about 10,000 hours.¹²

The more recently introduced phosphorescent metal-organic complexes¹³ allow one, in principle, to reach 100% IQE by overcoming the limits imposed by branching between spin states of different multiplicities. Red and green OLEDs based on phosphorescent iridium complexes showed EQEs above 20% with a turn-on voltage below 3 V.¹⁴ More recently, green-emitting OLEDs with an optimized light out-coupling design demonstrated an EQE of 63%.¹⁵ Blue phosphorescent OLEDs also exhibit

performance competing with that of the best devices based on blue fluorescent molecules, exhibiting EQEs as high as 14%.¹⁶

Despite impressive advances in the OLED field, there are a few drawbacks of this technology that might prevent its widespread use in commercial products. One problem is poor cost-efficiency, which is at least partially due to the complexity of the necessary device architecture, which requires processing involving multiple thermal deposition steps. Another problem is their limited stability, particularly for deep-red and blue phosphorescent OLEDs. While being greatly improved over the years, it still does not meet the standards employed in high-end devices. Furthermore, the color purity of OLEDs, that is, the width of the emission band, is inferior to that of conventional semiconductor LEDs. Specifically, the emission full width at half maximum of OLEDs is typically greater than 40 nm (Figure 1, dashed lines), while it is less than 30 nm for conventional LEDs.

A promising class of emissive materials for low-cost yet efficient LEDs is chemically synthesized nanocrystal quantum dots (QDs). These luminescent nanomaterials feature size-controlled tunable emission wavelengths, combined with improvements in both color purity (Figure 1, solid lines) as well as stability and durability over organic molecules. At the same time, as with organic materials, colloidal QDs can be fabricated and processed via inexpensive solution-based techniques compatible with lightweight, flexible substrates.^{17–19}

Similar to other semiconductor materials, colloidal QDs feature almost continuous above-band-edge absorption and a narrow emission spectrum at a near-band-edge energy. Distinct from bulk semiconductors, however, the optical spectra of QDs depend directly on their size. Specifically, their emission color can be continuously tuned from the infrared (IR) to ultraviolet

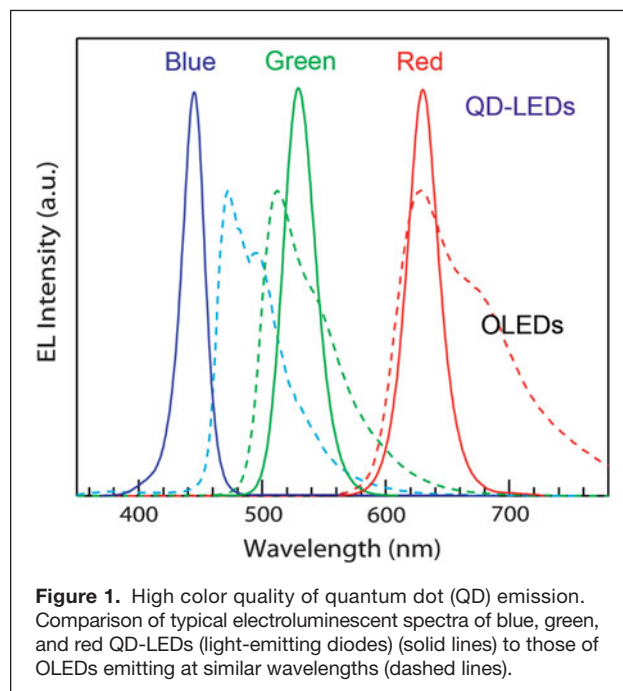


Figure 1. High color quality of quantum dot (QD) emission. Comparison of typical electroluminescent spectra of blue, green, and red QD-LEDs (light-emitting diodes) (solid lines) to those of OLEDs emitting at similar wavelengths (dashed lines).

(UV) by varying QD size and/or composition.^{19–22} The wide-range spectral tunability is combined with high photoluminescence (PL) quantum yields (QYs) that approach unity in well-passivated structures. These unique properties of the QDs have been extensively explored for realizing various devices such as LEDs,²³ lasers,²⁴ solar cells,²⁵ and photodetectors.²⁶

Among the large number of prospective applications, the use of QDs in light-emitting devices is of particular interest due to a potentially large and immediate impact on display and lighting markets. In the last decade, vigorous research has explored the applications of QDs in light-emitting systems.^{27–34} As a result of these efforts, numerous types of QD-LEDs have been successfully demonstrated,^{28,35–39} and their performance has been improved up to a point where it nearly meets the requirements for commercial products. Thus, while QD-LEDs still represent an emerging technology, they are expected to compete with OLEDs in the very near future.

This remarkable progress in the QD-LED field would be impossible without recent advances in QD synthesis and in the understanding of their fundamental photophysical properties. In the next sections, we discuss the factors that limit the emission efficiency of QD-LEDs, as well as approaches for controlling these factors via appropriate engineering of the internal structure of the QDs, their interfaces, as well as the architecture of an entire device.

Mechanisms for nonradiative losses in quantum dots

One factor limiting the performance of QD-LEDs is associated with nonradiative recombination within the QD emitters. Later, we consider nonradiative processes such as carrier recombination via surface defects, including hot-electron trapping (discussed in the context of QD “blinking”) and nonradiative losses due to exciton transfer. We also analyze nonradiative Auger decay in the presence of extra charges and, specifically, the implications of asymmetry between recombination pathways in positively and negatively charged QDs.

Recombination via surface defects in isolated QDs and QD films

Light emission from QDs can be activated either via photoexcitation, which leads to PL, or electrical charge injection, which produces EL. The EL efficiency of QDs incorporated into LEDs is directly linked to their PL QY. A typical (but not universal) trend is that QDs with a higher PL QY produce more efficient EL. Therefore, the initial evaluation of QDs for their suitability for LED applications is usually conducted on the basis of spectroscopic studies of QD PL efficiencies and the mechanisms for nonradiative losses responsible for non-unity values of QY.

One such mechanism is recombination of “relaxed” band-edge electrons and holes via surface defects (**Figure 2a**).⁴⁰ This is an important channel for nonradiative decay due to the very large surface-to-volume ratio of a QD. For example, in CdSe dots with radius $R = 1.5$ nm, as many as ~35% of atoms reside on the dot surface.^{41,42} If we denote the rates of radiative and surface related recombination as k_r and k_{nr} , respectively, the PL QY (Q) can be expressed as $Q = k_r / (k_r + k_{nr})$, while the PL lifetime is $\tau_{PL} = (k_r + k_{nr})^{-1}$. In addition to reducing emission efficiencies, surface traps can also act as active sites for photochemical degradation of QDs,⁴¹ which limits the operational lifetime of the LEDs.

For the past two decades, rapid advances have been made in the structural engineering of QDs for reducing detrimental effects of surface recombination. The most common strategy involves overcoating a QD with an external shell of a wider-gap semiconductor (e.g., CdS or ZnS in the case of CdSe dots). In these core-shell QDs, electron and hole wave functions are confined to the core domain and thus are better isolated from defects on the QD surface, which leads to enhanced PL QY and improved photochemical stability.^{43–47} Recent approaches have involved the use of more sophisticated structures (e.g., CdS/ZnS, ZnSe/ZnS, CdS/ZnCdS/ZnS multi-shells^{46,48,49} or Cd_{1-x}Zn_xSe_{1-y}S_y compositionally graded shells^{50,51}) that demonstrate near-unity PL QYs and high photochemical stability, which approaches the standards of practical light-emission applications.

While these considerations have been applied to isolated QDs (e.g., dilute solution samples), they can be extended

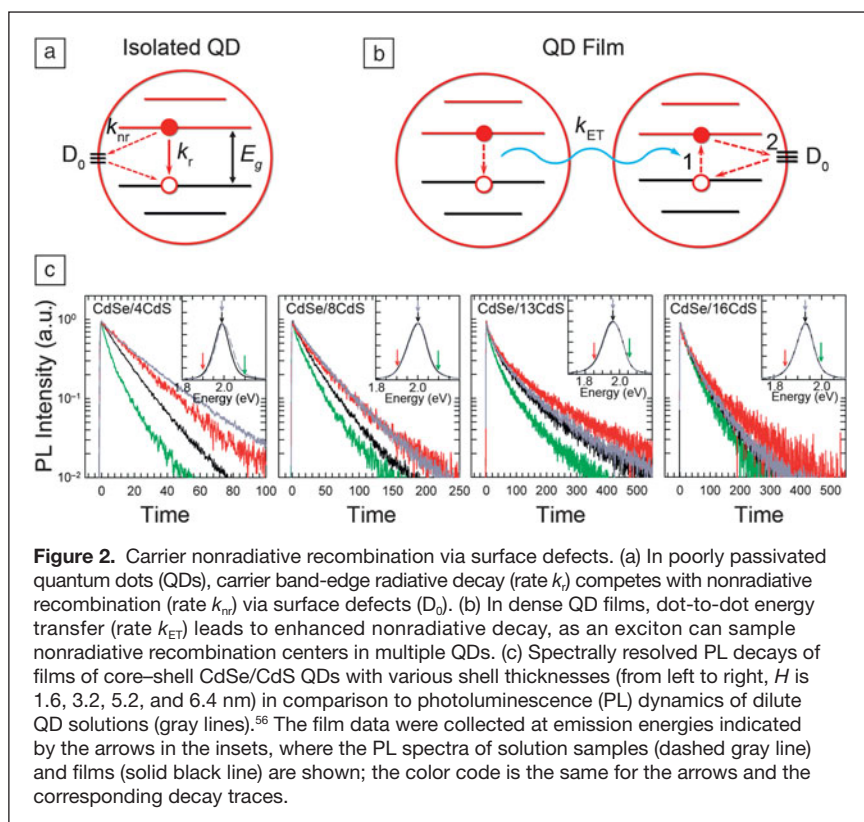


Figure 2. Carrier nonradiative recombination via surface defects. (a) In poorly passivated quantum dots (QDs), carrier band-edge radiative decay (rate k_r) competes with nonradiative recombination (rate k_{nr}) via surface defects (D_0). (b) In dense QD films, dot-to-dot energy transfer (rate k_{ET}) leads to enhanced nonradiative decay, as an exciton can sample nonradiative recombination centers in multiple QDs. (c) Spectrally resolved PL decays of films of core-shell CdSe/CdS QDs with various shell thicknesses (from left to right, H is 1.6, 3.2, 5.2, and 6.4 nm) in comparison to photoluminescence (PL) dynamics of dilute QD solutions (gray lines).⁵⁶ The film data were collected at emission energies indicated by the arrows in the insets, where the PL spectra of solution samples (dashed gray line) and films (solid black line) are shown; the color code is the same for the arrows and the corresponding decay traces.

to dense QD films typically used as the active layers of LEDs. In this case, the role of surface recombination is amplified because of energy transfer (ET), which allows for a given exciton to sample trap centers in multiple QDs within the ET distance (the distance for which the ET time is equal to the exciton recombination time in an isolated QD) (Figure 2b). In QDs, ET typically leads to a red shift of the PL peak, which is accompanied by acceleration of PL decay, especially pronounced on the blue side of the emission spectrum, which corresponds to smaller dots in the sample.^{52,53} The emitting dipole of these dots readily couples to the strong absorption dipole of bigger dots, which leads to a migration of excitons to the largest QDs in the ensemble.

For closely spaced CdSe QDs (e.g., in dense Langmuir–Blodgett films⁵⁴), the ET time can be as short as ca. 100 ps. It is slower in commonly used films made via drop casting, dip coating, or spin coating; however, even in this case, the characteristic time of ET (typically a few nanoseconds⁵²) is faster than the radiative lifetime (~20 ns for CdSe QDs⁵⁵). Therefore, it can compete with radiative recombination, leading to reduced PL QYs compared to solution samples.

To quantify this reduction, we consider a simplified situation where the QD ensemble comprises only two types of dots: “bright” with PL QY equal to unity and “dark” with a zero QY. The corresponding QY (Q_0) of a non-interacting QD ensemble is simply defined by the fraction of “bright” dots. If this sample is assembled in a film, the exciton generated in a “bright” QD can either recombine within it (radiatively under our assumptions) or migrate to a different dot with the total rate k_{ET} . Since the acceptor dot can be nonemissive (“dark”) with a probability $(1-Q_0)$, each ET step leads to the reduction in the PL QY. For the infinite number of these steps, the overall PL QY can be found from

$$Q_\infty = Q_0 \left[\frac{k_r}{k_r + k_{ET}} \right] \left\{ 1 + Q_0 k_{ET} / (k_r + k_{ET}) + [Q_0 k_{ET} / (k_r + k_{ET})]^2 + \dots \right\}, \quad (1)$$

which yields

$$Q_\infty = Q_0 k_r / [k_r + k_{ET} (1 - Q_0)]. \quad (2)$$

If, for example, we consider a sample with $Q_0 = 0.8$ and typical values of radiative (0.05 ns^{-1}) and ET (0.5 ns^{-1}) rates, we obtain $Q_\infty = 0.27$, three times lower than the original QY. This estimation shows that even highly luminescent solution samples may experience a significant reduction in effective emission efficiency upon processing into a film. This highlights the need for designing QD samples that feature not only high emission efficiencies in solution form, but also suppressed ET when they are assembled into dense films.

A recent study of LEDs based on CdSe/CdS QDs⁵⁶ has demonstrated that an increase in the shell thickness (H) leads to a progressive increase in the LED EQE, which among other

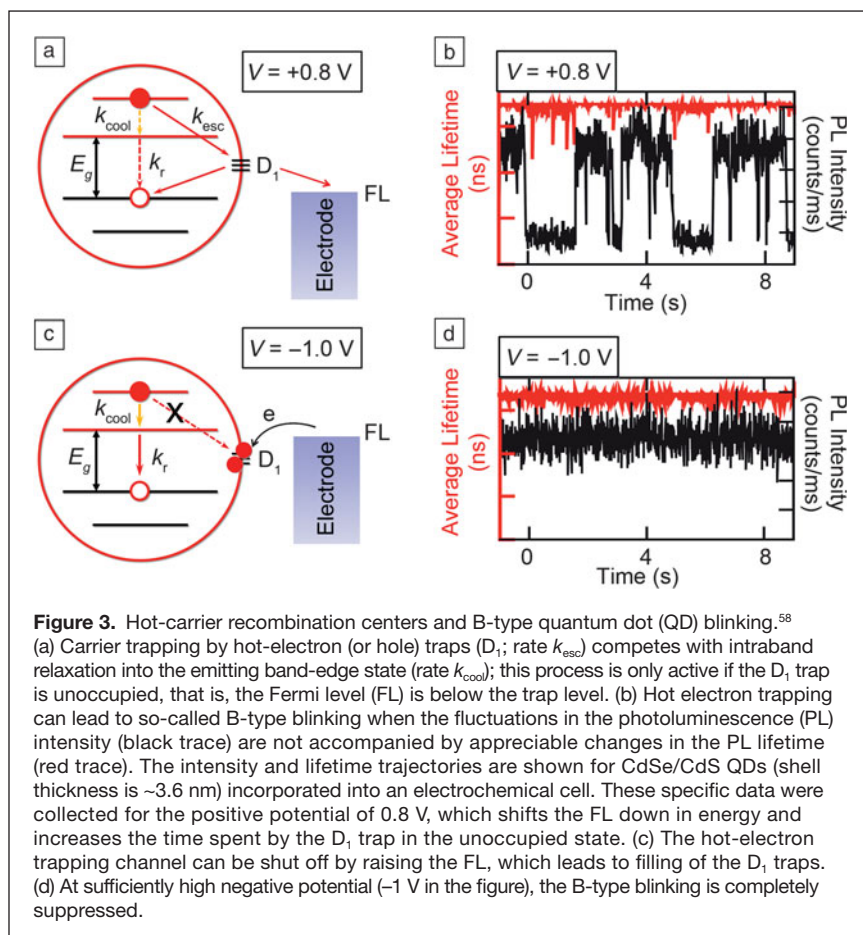
factors was attributed to suppression of exciton quenching by ET. Figure 2c displays the effect of increasing shell thickness on PL dynamics of QD film versus solution samples. As was pointed out earlier, the PL decay measured on the blue side of the emission band of the QD films represents a qualitative measure of the ET time. As evident from Figure 2c, this decay becomes progressively slower with increasing H , and in the thickest-shell sample ($H = 6.4 \text{ nm}$), it is essentially the same as in the solution of non-interacting QDs. This suggests a nearly complete suppression of ET due to the thick shells acting as spacers separating the cores of the donor and the acceptor QDs involved in the ET process. The observed ET suppression is well correlated with the increase in the EL EQE of QD films incorporated into LEDs.⁵⁶

Hot carrier trapping/recombination and B-type QD blinking

More recently, there has been increasing evidence from both single-dot^{57,58} and ensemble^{59–61} measurements of the importance of nonradiative recombination involving surface/interface trapping of “hot,” unrelaxed carriers (Figure 3a). In the absence of other nonradiative channels, the PL QY due to hot electron trapping/recombination can be described by $Q = k_{cool} / (k_{cool} + k_{esc})$, where k_{esc} is the rate of hot-electron escape from the QD, and k_{cool} is the rate of intraband relaxation to the emitting band-edge state. A distinct feature of this mechanism is that while leading to reduced PL intensity, it does *not* change the emission lifetime, which under the previous assumption is defined by radiative decay of a band-edge exciton. If both channels (band-edge and hot-carrier trapping) are active, the resulting QY can be expressed as $Q = k_{cool} k_r / [(k_{cool} + k_{hot})(k_r + k_{nr})]$.

Hot-carrier trapping has been invoked to explain photocharging of QDs under excitation with above-bandgap photons,^{59–61} and recently was used to explain one of the regimes (so-called B-type blinking) of PL intermittency (that is, switching of a QD between high- and low-emissivity states) observed in single-dot measurements.⁵⁸ This regime is characterized by strong fluctuations in PL intensity that are not accompanied by any significant variations in PL lifetime. This is exactly the signature of a recombination channel due to hot-electron traps, which randomly turns on and off due to fluctuations in the traps' occupancy.⁵⁸

Strong support for this model was provided by demonstrations of the control of B-type blinking by applied potential for QDs incorporated into an electrochemical cell.⁵⁸ Specifically, it was observed that under positive bias, which corresponded to a lower Fermi level, the low-emissivity (OFF) periods were extended due to increasing time spent by the hot-electron trap in the unoccupied, active state (Figure 3b). On the other hand, under sufficiently negative potential, the B-type OFF periods were completely suppressed, as expected for the situation of a higher Fermi level, which leads to filling (that is, blocking) of hot-electron traps (Figure 3c–d). This explanation of B-type blinking suppression due to filling of electron-accepting trap sites is consistent with previous observations of PL enhancement



and blinking suppression due to electron-donating molecules^{62,63} and n -doped substrates.⁶⁴

As with band-edge trapping, the B-type hot-electron trapping can be suppressed by growing a sufficiently thick shell. The analysis of blinking behaviors for CdSe/CdS QDs⁵⁸ indicates that the occurrence of B-type blinking is reduced as the thickness of the CdS shell is increased, and it is completely eliminated in samples with shells comprising more than 15 monolayers of CdS. These thick-shell QDs (often referred to as giant- or g-QDs) were either nonblinking or exhibited so-called A-type blinking due to charging/discharging of the QD core.⁵⁸ Interestingly, a closer inspection of lifetime trajectories indicated that some of the nonblinking dots, while showing stable emission intensity, were still characterized by significant fluctuations of the PL lifetime (“lifetime blinking”⁵⁷) due to switching between neutral exciton and negative trion states; the charged state was highly emissive because of suppressed Auger recombination in this type of structure (as discussed in the following sections).

Nonradiative Auger recombination of charged excitons

An important mechanism for nonradiative losses in QDs is associated with Auger recombination of multicarrier states,

that is, states involving more than one exciton. The simplest of these states are singly charged excitons, or negative (Figure 4a) and positive (Figure 4b) trions (X^- and X^+ , respectively). In addition to radiative or extrinsic defect-related processes, charged excitons can decay via nonradiative Auger recombination, a process in which the energy of an electron–hole pair is converted not into a photon but instead is transferred to a third carrier. This process is inefficient in bulk forms of wide-gap semiconductors, but due to relaxation of momentum conservation,⁶⁵ it is extremely efficient in QDs, where it is characterized by a short (a few ps to hundreds of ps) time constant (τ_A) that exhibits direct scaling with QD volume (V), $\tau_A \propto V$, sometimes referred to as “ V -scaling.”^{66,67}

Charged states can be created within QDs under light exposure (photocharging^{59–61}), due to direct electrical contact with a metal or semiconductor substrate, or can arise because of an imbalance between electron and hole injection currents in LED devices. There is ample evidence that charging has a significant detrimental impact on the performances of light-emitting systems relying on QDs.^{41,58,67–82} To quantify the effect of extra charges on QD emission, we assume that the radiative decay rate scales linearly with the number of available recombination pathways, that is, it is directly

proportional to the product of the electron (N_e) and the hole (N_h) occupancy of the QD:^{83,84}

$$k_r(N_e; N_h) = N_e N_h k_{\text{tr}}, \quad (3)$$

where k_{tr} is the radiative decay rate of a neutral exciton ($N_e = 1$; $N_h = 1$). Based on this expression, the radiative rates of negative and positive trions are $k_{\text{tr}} = k_{\text{tr}} = 2k_1$ and corresponding PL QYs are

$$Q_{-1} = 2k_1 / (2k_1 + k_{-1A}) \text{ and } Q_{+1} = 2k_1 / (2k_1 + k_{+1A}). \quad (4)$$

Since in standard core-only or thin-shell QDs the rate of Auger decay is several orders of magnitude higher than the radiative decay rate, the expression for QYs can be approximated by $Q_{-1} \approx 2k_1/k_{-1A}$ and $Q_{+1} \approx 2k_1/k_{+1A}$.

The trion Auger lifetimes can be inferred from spectroscopic measurements of a neutral biexciton (a state comprising two electrons and two holes) decay rate (k_{2A}), which is related to the X^- and X^+ decay rates as $k_{2A} = 2(k_{-1A} + k_{+1A})$. In core-only QDs that feature mirror symmetric conduction and valence bands, $k_{-1A} = k_{+1A} = k_{2A}/4$. Such a situation is realized, for example, in PbSe QDs for which the observed trion Auger lifetime is indeed approximately four times longer than that of

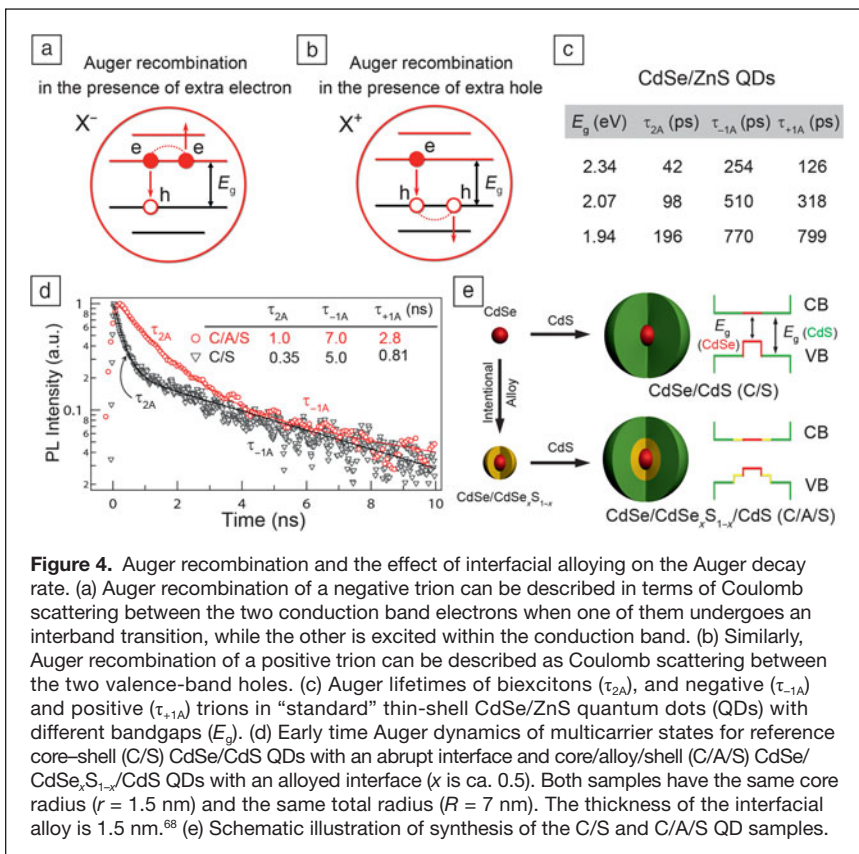


Figure 4. Auger recombination and the effect of interfacial alloying on the Auger decay rate. (a) Auger recombination of a negative trion can be described in terms of Coulomb scattering between the two conduction band electrons when one of them undergoes an interband transition, while the other is excited within the conduction band. (b) Similarly, Auger recombination of a positive trion can be described as Coulomb scattering between the two valence-band holes. (c) Auger lifetimes of biexcitons (τ_{2A}), and negative (τ_{-1A}) and positive (τ_{+1A}) trions in “standard” thin-shell CdSe/ZnS quantum dots (QDs) with different bandgaps (E_g). (d) Early time Auger dynamics of multicarrier states for reference core-shell (C/S) CdSe/CdS QDs with an abrupt interface and core/alloy/shell (C/A/S) CdSe/CdSe_xS_{1-x}/CdS QDs with an alloyed interface (x is ca. 0.5). Both samples have the same core radius ($r = 1.5$ nm) and the same total radius ($R = 7$ nm). The thickness of the interfacial alloy is 1.5 nm.⁶⁸ (e) Schematic illustration of synthesis of the C/S and C/A/S QD samples.

a biexciton (τ_{2A}). Recent measurements of chemically doped samples⁸⁵ indicate that in PbSe QDs with $E_g = 0.76$ eV ($R = 3.85$ nm), the X^- Auger lifetime is 360 ps, very close to the expected value of 416 ps predicted from the measured τ_{2A} of 104 ps.

The symmetry between the X^- and X^+ recombination pathways can be distorted in QDs of II–VI semiconductors due to the significant difference between the conduction and valence bands. Specifically, a much higher density of valence-band states favors the positive trion Auger recombination channel (Figure 4b) for which the energy conservation requirement is easier to meet. Recent measurements⁸⁶ have evaluated the biexciton and negative trion Auger lifetimes in thin-shell CdSe/ZnS QDs using time-resolved picosecond cathodoluminescence. The results of these measurements are summarized in Figure 4c (τ_{+1A} is derived from the measured τ_{-1A} and τ_{2A}). One can see that in larger dots ($E_g = 1.94$ eV), τ_{+1A} and τ_{-1A} are close to each other (770 ps and 799 ps, respectively). However, as the dot size is decreased, the X^- Auger pathway gets progressively suppressed due to increasing separation between the conduction band states, so that in QDs with $E_g = 2.34$ eV, the Auger lifetime of the positive trion (126 ps) is ca. twice as fast as that of the negative trion (254 ps).

The asymmetry between the X^- and X^+ recombination pathways is further enhanced in core-shell structures that feature a significant difference in effective localization radii (defined by the spatial extent of electronic wave functions) of electrons

(R_c) and holes (R_h). One example is thick-shell CdSe/CdS g-QDs.^{70,75} In these dots, the electron is delocalized over the entire nanostructure, while the hole is confined to the smaller core, and hence, R_c is much greater than R_h . This enhances the Auger decay rate of the positive versus negative trion due to increased probability of hole-hole scattering events (involved in the X^+ decay channel; Figure 4b) compared to electron-electron scattering (involved in the X^- decay channel; Figure 4a). For example, based on a recent experimental study of core-shell CdSe/CdS QDs,⁶⁸ in samples with core radius $r = 1.5$ nm and $H = 5.5$ nm, $\tau_{-1A} = 5$ ns and $\tau_{2A} = 0.35$ ns (inset of Figure 4d). These values yield $\tau_{+1A} = 0.81$ ns, which suggests a very significant asymmetry between the X^- and X^+ Auger decay channels with $\tau_{-1A} \approx 6\tau_{+1A}$.

On the basis of the previous analysis of trion Auger lifetimes, we can estimate their emission efficiencies. Using the data obtained for standard thin-shell CdSe/ZnS QDs and assuming a 20 ns neutral-exciton radiative time constant,⁵⁵ we estimate that for the sample with $E_g = 2.34$ eV (Figure 4c), the negative trion PL QY is only 2.5%, and this is even lower (1.3%) for positive trions. The trion QY is increased for larger samples (e.g., $Q_{-1} \approx Q_{+1} \approx 7\%$ for QDs with $E_g = 1.94$ eV); however, it is still below 10%.

These estimations indicate that QD charging can greatly reduce emission efficiency and hence the EQE of LEDs. As was shown in previous work,^{72,73,82} the use of g-QDs with an ultra-thick CdS shell allows for significant suppression of Auger recombination, which translates into increased trion lifetimes and hence emission yields; this was cited as one of the reasons for improved performance of LEDs comprising CdSe/CdS g-QDs.⁵⁶ Indeed, for the thick-shell CdSe/CdS sample in Figure 4d, we estimate that the negative trion PL QY is ~20%, which is considerably higher than in standard dots. However, we would like to point out that because of a significant asymmetry between the X^- and X^+ Auger pathways in these structures, the X^+ QY is still low (~3%) and is comparable to that in standard QDs. This observation highlights the fact that while charging is in general detrimental to LED performance, the presence of extra holes is especially harmful, as positive trion lifetimes in many types of II–VI QDs can be significantly shorter than the lifetimes of negative trions.

Suppression of Auger recombination via “interface engineering”

The previous analysis indicates that Auger recombination represents a serious impediment to the realization of high emission efficiency in situations where the formation of multicarrier states is difficult to avoid, such as high-intensity (and/or high-photon energy) optical excitation or electrical pumping

when even a slight imbalance in electron and hole currents can lead to QD charging with extra carriers. Therefore, the development of approaches for suppression of Auger decay could greatly benefit LEDs.

As was mentioned earlier, one approach to reducing Auger decay rates involves overcoating CdSe cores with exceptionally thick CdS shells.^{72,73} Originally, these structures were expected to exhibit suppressed Auger recombination based on V -scaling arguments and the reduced electron–hole overlap due to a considerable mismatch in effective radii of electron and hole localization ($R_e \gg R_h$). However, as was pointed out in Reference 72, these factors alone could not explain the observation of very rapid lengthening of τ_{2A} with increasing shell thickness, suggesting that other structural characteristics of the QD such as the properties of its interfaces might play an important role in Auger recombination.

Indeed, calculations by Cragg and Efros⁷¹ as well as a follow-up theoretical study by Climente et al.⁸⁷ have suggested that the shape of the confinement potential also has a significant effect on the Auger decay rate. Specifically, these studies demonstrated that by smoothing the confinement potential (via, e.g., alloying the interfacial layer), one can reduce the overlap between the initial and the final state of the carrier excited during Auger recombination and thus achieve an orders-of-magnitude reduction in the rate of this process.

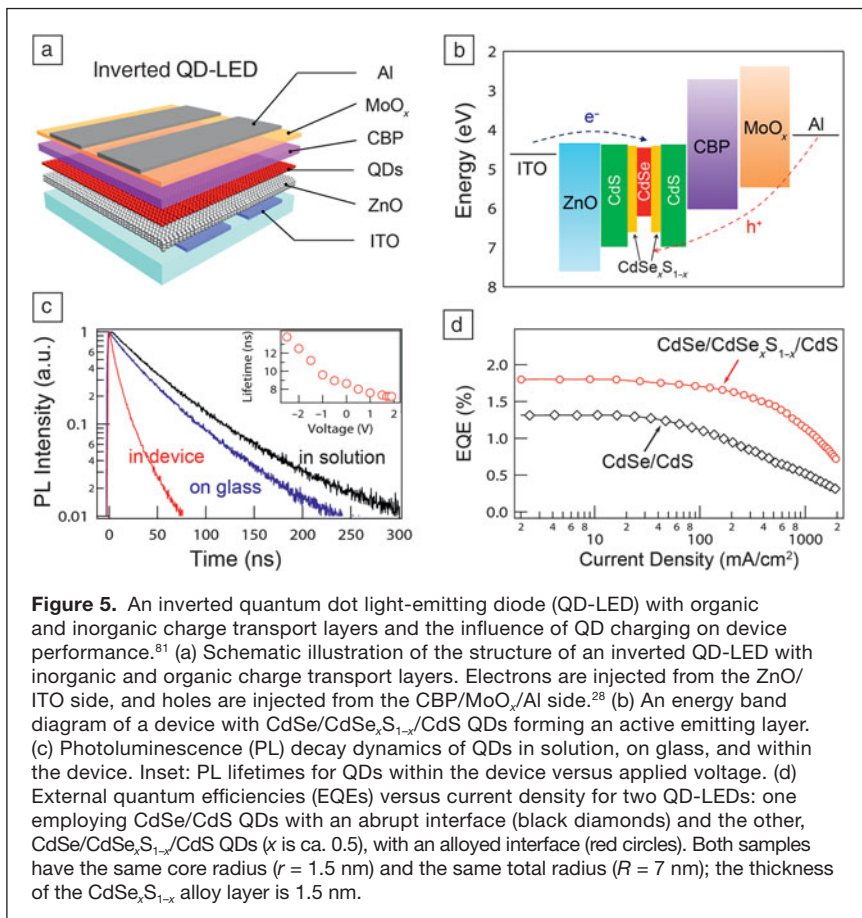
Recently, the problem of the effect of interfacial alloying on Auger recombination was directly addressed by studying carrier dynamics in core–shell CdSe/CdS QDs with a well-defined CdSe_{*x*}S_{1-*x*} alloy incorporated between the core and the shell (Figure 4d–e).^{68,88} These studies were enabled by a novel synthesis method,⁶⁸ allowing much faster growth of a thick CdS shell compared to a more traditional successive ionic layer adsorption and reaction (SILAR) method,^{70,75,89} which was essential for avoiding unintentional alloying at the CdSe/CdS interface. Using this method, it was possible to synthesize structures with either a sharp core–shell boundary (C/S QDs) or with a CdSe_{*x*}S_{1-*x*} alloy layer incorporated between the core and shell (C/A/S QDs); see Figure 4e.⁶⁸

Side-by-side studies of spectroscopic properties of these QDs⁶⁸ indicated that the incorporation of the interfacial alloy layer did not significantly influence either spectra or dynamics of single excitons; however, it had a profound effect on multicarrier dynamics and PL QY of multicarrier states. For example, a direct comparison of the C/S and C/A/S samples (alloy layer thickness $L = 1.5$ nm and $x \approx 0.5$) with the same core radius ($r = 1.5$ nm) and the same total size ($R = 7$ nm) indicates that the Auger lifetimes are systematically longer for the C/A/S QDs (Figure 4d). While observed

for both X⁻ and X⁺ states, lifetime lengthening is especially pronounced for positive trions (2.8 ns versus 0.81 ns for the C/A/S and the C/S samples, respectively), which results in considerable improvement of PL QY (~12% versus ~3% in the sample without the interfacial alloy). A stronger effect of interfacial alloying on X⁺ dynamics is expected based on the fact that it primarily affects the shape of the hole confinement potential. As discussed in the next section, the use of alloyed dots in LEDs allows one to improve their EQE compared to core–shell structures with a sharp interface, and this improvement is especially pronounced for high injection currents when the EQE loss due to Auger decay is particularly significant.

Effects of charging in LEDs and high-intensity roll-off of LED efficiency

When QDs are incorporated into devices, they can acquire a net charge due to interactions with electrodes and/or charge transport layers. Recently, this effect has been studied⁸¹ using the so-called inverted LED architecture, where a QD active layer is sandwiched between an inorganic metal-oxide electron transport layer and an organic hole transport layer based on conjugated molecules (Figure 5a). This architecture has been previously applied in high-performance devices^{27–29,81,90} that feature low turn-on voltage (nearly the same as the QD bandgap), high external EQEs at practical brightness



(100–1000 cd/m²), and good operational stability (half lifetime ~500 hr).^{28,29}

Figure 5b shows an energy diagram of a device utilizing alloyed CdSe/CdSe_xS_{1-x}/CdS QD emitters (same samples as in Figure 4d–e) and an *n*-type colloidal ZnO electron injection layer assembled on an indium-tin-oxide (ITO) cathode together with a 4,4'-bis(*N*-carbazolyl)-1,1'-biphenyl (CBP) hole conducting layer separated from the Al anode by a thin MoO_x spacer.⁸¹ Due to the energetic proximity of the QD conduction-band level to the Fermi level of the ITO cathode, electron injection from ITO into QDs occurs spontaneously at zero bias, as indicated by a direct comparison of PL dynamics for dots assembled on the “passive” glass substrate versus the dots on the ITO/ZnO electrode (Figure 5c). In the former case, the PL dynamics are nearly the same as for isolated QDs in solution, while in the latter, the dynamics are significantly faster due to Auger recombination of the negative trion state arising from the combination of a photoexcited exciton and an injected electron. Indeed, the measured PL lifetime of 8.5 ns is very close to the Auger recombination time of a negative trion inferred from spectroscopic studies of QD solutions (inset of Figure 4d).

The fact that the observed changes in carrier decay are due to excess electrons is confirmed by the observed changes in the PL lifetime as a function of applied bias (inset of Figure 5c). Under reverse bias, which makes electron injection less favorable, the PL decay becomes slower as expected for the situation in which a QD fluctuating between the charged and the neutral state spends an increasing amount of time in the neutral state.⁵⁸ On the other hand, the PL dynamics get faster under direct bias due to increasing contribution from doubly negatively charged excitons.⁵⁸

A distinct asymmetry in the response to negative versus positive bias also indicates that the observed changes in PL dynamics are not significantly altered by effects that are independent of the electric-field direction, such as field-induced spatial separation between a photo-generated electron and a hole with a QD.⁹⁰ These observations also lead to the important conclusion that a likely reason for the efficiency roll-off (also known as efficiency droop) at large currents is the increasing degree of dot charging with excess electrons, which leads to increasing nonradiative carrier losses due to Auger recombination. Indeed, if we compare LEDs fabricated using core-shell CdSe/CdS QDs to those made using alloyed CdSe/CdSe_xS_{1-x}/CdS dots, which exhibit suppressed Auger recombination (Figure 4d–e), we observe that the onset of the EQE roll-off is considerably higher in alloyed QDs than in structures with a sharp core-shell interface (Figure 5d).

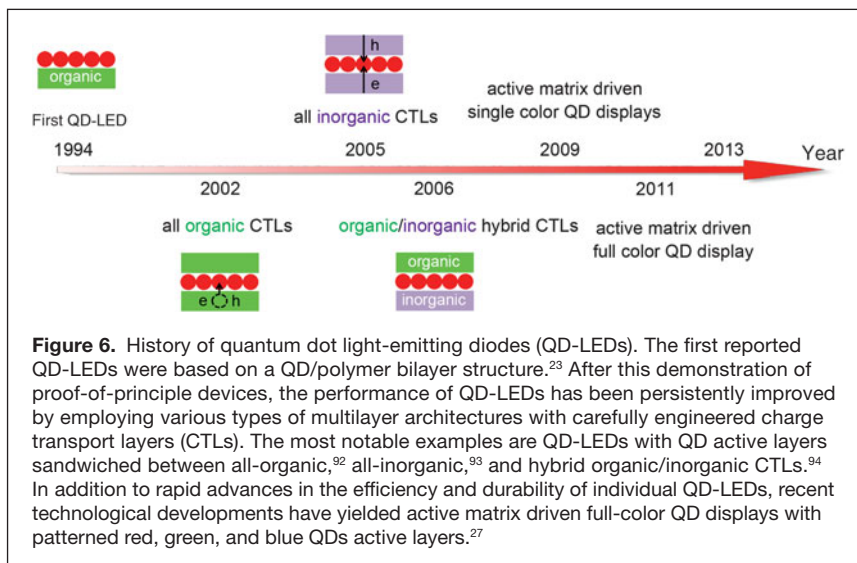
Summary and outlook

QD-LEDs have advanced tremendously over the past two decades, and progress has been

especially fast recently due to significant improvements in the quality of QD materials as well as advances in the architecture of the devices. As illustrated in **Figure 6**, over the years, the QD-LED architecture has evolved from proof-of-principle polymer-QD bilayer structures to modern devices employing direct charge injection from finely tuned electron and hole transport layers (see, e.g., Figure 5a). Recent refinements of this latter architecture have led to the demonstration of devices with a peak EQE of 18%,²⁹ which is near the theoretical maximum of 20%. At the same time, parallel engineering efforts have demonstrated the feasibility of full-color active-matrix-driven QD displays with patterned red, green, and blue QDs active layers.²⁷

As in the field of OLEDs, an important outstanding challenge in the field of QD-LEDs is the stability of device operation, especially for high injection currents. For example, the record efficiency devices of Reference 29 were able to maintain the highest EQE for only less than one hour. The reasons for the instability likely relate to both chemical (photochemical) degradation of the QDs as well as photophysical effects. As discussed in the previous sections, growing evidence suggests a detrimental effect of charging on LED performance. The presence of excess charges in the QDs might lead to both reversible degradation of the LED efficiency due to Auger recombination as well as irreversible changes due to activation of chemical reactions at the QD surface and/or in the ligand shell.⁴¹ As discussed earlier, charging is also a likely reason for the significant efficiency roll-off observed for high driving currents.^{28,29,81}

These considerations imply that realization of high-performance LEDs requires QD materials that exhibit high emission efficiencies not only in the single-exciton but also multi-carrier regimes. Two examples of such structures discussed in this article are thick-shell CdSe/CdS g-QDs^{70,73,75} and recently demonstrated CdSe/CdSe_xS_{1-x}/CdS QDs, with an intermediate alloyed layer introduced for suppression of



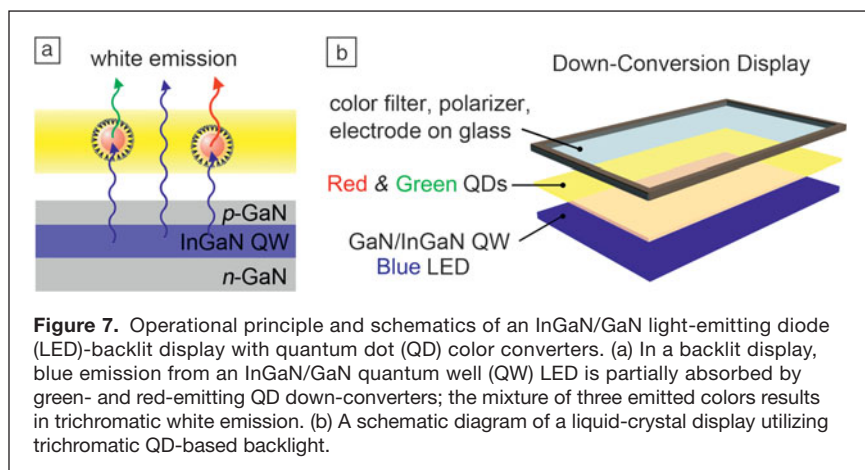


Figure 7. Operational principle and schematics of an InGaN/GaN light-emitting diode (LED)-backlit display with quantum dot (QD) color converters. (a) In a backlit display, blue emission from an InGaN/GaN quantum well (QW) LED is partially absorbed by green- and red-emitting QD down-converters; the mixture of three emitted colors results in trichromatic white emission. (b) A schematic diagram of a liquid-crystal display utilizing trichromatic QD-based backlight.

Auger recombination.⁶⁸ Other reported structures that demonstrated suppressed Auger decay include $\text{Cd}_x\text{Zn}_{1-x}\text{Se}/\text{ZnSe}$ ⁷⁸ and CdTe/CdSe .⁹¹

The detrimental effects of charging can also be reduced via a careful choice/design of charge transport layers for achieving balanced electron and hole injection currents. “Electrode engineering” can also help lower the operational voltage, and, as a result, the strength of the electric field within the QD layer. This might also help mediate the problem of efficiency roll-off, as some studies suggest that in certain cases, this roll-off can be attributed to the reduction of the QD emission rate due to field-induced spatial separation between electrons and holes.⁹⁰

While the performance of QD-LEDs is quickly approaching industry standards for lighting and displays, the first commercial applications of QDs will likely utilize them as down-converters. In such devices (e.g., backlit units), QDs are not excited by passing current, but instead are excited optically by absorbing blue radiation from InGaN/GaN quantum well LEDs before reemitting green or red light (Figure 7a–b).^{30–34} Recently, Sony Corporation has announced that it plans to incorporate QD-based down-conversion white LEDs as a backlight unit into their LCD television sets. Similar directions are being pursued by other big companies such as Samsung, LG, etc. Given these recent advances, it is reasonable to expect that the very exciting moment when the first QD product appears on the market is just around the corner.

Acknowledgments

This work was supported by the Chemical Sciences, Biosciences, and Geosciences Division of Office of Science, Office of Basic Energy Sciences, US Department of Energy.

References

1. E.F. Schubert, *Light-Emitting Diodes* (Cambridge University Press, Cambridge, UK, 2006).
2. S. Schols, *Device Architecture and Materials for Organic Light-Emitting Devices: Targeting High Current Densities and Control of the Triplet Concentration* (Springer, London, UK, 2011).
3. F. So, *Organic Electronics: Materials, Processing, Devices and Applications* (CRC Press, Boca Raton, FL, 2009).

4. A.B. Tamayo, B.D. Alleyne, P.I. Djurovich, S. Lamansky, I. Tsyba, N.N. Ho, R. Bau, M.E. Thompson, *J. Am. Chem. Soc.* **125**, 7377 (2003).
5. S. Lamansky, P. Djurovich, D. Murphy, F. Abdel-Razzaq, H.-E. Lee, C. Adachi, P.E. Burrows, S.R. Forrest, M.E. Thompson, *J. Am. Chem. Soc.* **123**, 4304 (2001).
6. S.R. Forrest, M.L. Kaplan, P.H. Schmidt, *J. Appl. Phys.* **56**, 543 (1984).
7. J.H. Burroughes, D.D.C. Bradley, A.R. Brown, R.N. Marks, K. Mackay, R.H. Friend, P.L. Burns, A.B. Holmes, *Nature* **347**, 539 (1990).
8. G. Gustafsson, Y. Cao, G.M. Treacy, F. Klavetter, N. Colaneri, A.J. Heeger, *Nature* **357**, 477 (1992).
9. W.J. Begley, T.K.S.I. Hatwar, *SID Intl. Symp. Dig. Tech. Papers* **37**, 942 (2006).
10. H. Kuma, J. Jinde, M. Kawamura, *SID Intl. Symp. Dig. Tech. Papers* **38**, 1504 (2007).
11. M. Ricks, J.R. Vargas, K.P. Klubek, *SID Intl. Symp. Dig. Tech. Papers* **38**, 830 (2007).
12. D. Kondakov, *SID Intl. Symp. Dig. Tech. Papers* **39**, 617 (2008).
13. M.A. Baldo, D.F. O'Brien, Y. You, A. Shoustikov, S. Sibley, M.E. Thompson, S.R. Forrest, *Nature* **395**, 151 (1998).
14. H. Sasabe, Y. Li, S. Su, T. Takeda, J. Kido, *Jpn. J. Appl. Phys.* **46**, 10 (2007).
15. Z.B. Wang, M.G. Helander, J. Qiu, D.P. Puzzo, M.T. Greiner, Z.M. Hudson, S. Wang, Z.W. Liu, Z.H. Lu, *Nat. Photonics* **5**, 753 (2011).
16. S.-J. Yeh, M.F. Wu, C.T. Chen, Y.H. Song, Y. Chi, M.H. Ho, S.F. Hsu, C.H. Chen, *Adv. Mater.* **17**, 285 (2005).
17. D.V. Talapin, J.S. Lee, M.V. Kovalenko, E.V. Shevchenko, *Chem. Rev.* **110**, 389 (2010).
18. A.P. Alivisatos, *Endeavour* **21**, 56 (1997).
19. V.I. Klimov, *Nanocrystal Quantum Dots* (CRC Press, New York, 2010).
20. L. Brus, *J. Phys. Chem.* **90**, 2555 (1986).
21. A.P. Alivisatos, *Science* **271**, 933 (1996).
22. C.B. Murray, C.R. Kagan, M.G. Bawendi, *Annu. Rev. Mater. Sci.* **30**, 545 (2000).
23. V.L. Colvin, M.C. Schlamp, A.P. Alivisatos, *Nature* **370**, 354 (1994).
24. V.I. Klimov, A.A. Mikhailovsky, S. Xu, A. Malko, J.A. Hollingsworth, C.A. Leatherdale, H.-J. Eisler, M.G. Bawendi, *Science* **290**, 314 (2000).
25. O.E. Semonin, J.M. Luther, S. Choi, H.-Y. Chen, J. Gao, A.J. Nozik, M.C. Beard, *Science* **334**, 1530 (2011).
26. G. Konstantatos, I. Howard, A. Fischer, S. Hoogland, J. Clifford, E. Klem, L. Levina, E.H. Sargent, *Nature* **442**, 180 (2006).
27. T.-H. Kim, K.-S. Cho, E.K. Lee, S.J. Lee, J. Chae, J.W. Kim, D.H. Kim, J.-Y. Kwon, G. Amarantunga, S.Y. Lee, B.L. Choi, Y. Kuk, J.M. Kim, K. Kim, *Nat. Photonics* **5**, 176 (2011).
28. J. Kwak, W.K. Bae, D. Lee, I. Park, J. Lim, M. Park, H. Cho, H. Woo, D.Y. Yoon, K. Char, S. Lee, C. Lee, *Nano Lett.* **12**, 2362 (2012).
29. B.S. Mashford, M. Stevenson, Z. Popovic, C. Hamilton, Z. Zhou, C. Breen, J. Steckel, V. Bulović, M. Bawendi, S. Coe-Sullivan, P.T. Kazlas, *Nat. Photonics* **7**, 407 (2013).
30. J. Lee, V.C. Sundar, J.R. Heine, M.G. Bawendi, K.F. Jensen, *Adv. Mater.* **12**, 1102 (2000).
31. E. Jang, S. Jun, H. Jang, J. Lim, B. Kim, Y. Kim, *Adv. Mater.* **22**, 3076 (2010).
32. H. Woo, J. Lim, Y. Lee, J. Sung, H. Shin, J.M. Oh, M. Choi, H. Yoon, W.K. Bae, K. Char, *J. Mater. Chem. C* **1**, 1983 (2013).
33. M. Achermann, M.A. Petruska, D.D. Koleske, M.H. Crawford, V.I. Klimov, *Nano Lett.* **6**, 1396 (2006).
34. M. Achermann, M.A. Petruska, S. Kos, D.L. Smith, D.D. Koleske, V.I. Klimov, *Nature* **429**, 642 (2004).
35. W.K. Bae, J. Kwak, J.W. Park, K. Char, C. Lee, S. Lee, *Adv. Mater.* **21**, 1690 (2009).
36. K.-S. Cho, E.K. Lee, W.-J. Joo, E. Jang, T.-H. Kim, S.J. Lee, S.-J. Kwon, J.Y. Han, B.-K. Kim, B.L. Choi, J.M. Kim, *Nat. Photonics* **3**, 341 (2009).
37. T.-H. Kim, K.-S. Cho, E.K. Lee, S.J. Lee, J. Chae, J.W. Kim, D.H. Kim, J.-Y. Kwon, G. Amarantunga, S.Y. Lee, B.L. Choi, Y. Kuk, J.M. Kim, K. Kim, *Nat. Photonics* **5**, 176 (2011).
38. W.K. Bae, J. Kwak, J. Lim, D. Lee, M.K. Nam, K. Char, C. Lee, S. Lee, *Nano Lett.* **10**, 2368 (2010).
39. J.M. Caruge, J.E. Halpert, V. Wood, V. Bulović, M.G. Bawendi, *Nat. Photonics* **2**, 247 (2008).
40. V.I. Klimov, D.W. McBranch, C.A. Leatherdale, M.G. Bawendi, *Phys. Rev. B* **60**, 13740 (1999).
41. M. Jones, S.S. Lo, G.D. Scholes, *Proc. Natl. Acad. Sci. U.S.A.* **106**, 3011 (2009).
42. J.M. Luther, J.M. Pietryga, *ACS Nano* **7**, 1845 (2013).
43. M.A. Hines, P. Guyot-Sionnest, *J. Phys. Chem.* **100**, 468 (1996).
44. B.O. Dabbousi, J. Rodriguez-Viejo, F.V. Mikulec, J.R. Heine, H. Mattoussi, R. Ober, K.F. Jensen, M.G. Bawendi, *J. Phys. Chem. B* **101**, 9463 (1997).

45. X. Peng, M.C. Schlamp, A.V. Kadavanich, A.P. Alivisatos, *J. Am. Chem. Soc.* **119**, 7019 (1997).
46. J.M. Pietryga, D.J. Werder, D.J. Williams, J.L. Casson, R.D. Schaller, V.I. Klimov, J.A. Hollingsworth, *J. Am. Chem. Soc.* **130**, 4879 (2008).
47. W.K. Bae, J. Joo, L.A. Padilha, J. Won, D.C. Lee, Q. Lin, W.-K. Koh, H. Luo, V.I. Klimov, J.M. Pietryga, *J. Am. Chem. Soc.* **134**, 20160 (2012).
48. D.V. Talapin, I. Mekis, S. Götzinger, A. Kornowski, O. Benson, H. Weller, *J. Phys. Chem. B* **108**, 18826 (2004).
49. R. Xie, U. Kolb, J. Li, T. Basché, A. Mews, *J. Am. Chem. Soc.* **127**, 7480 (2005).
50. W.K. Bae, K. Char, H. Hur, S. Lee, *Chem. Mater.* **20**, 531 (2008).
51. W.K. Bae, M.K. Nam, K. Char, S. Lee, *Chem. Mater.* **20**, 5307 (2008).
52. S.A. Crooker, J.A. Hollingsworth, S. Tretiak, V.I. Klimov, *Phys. Rev. Lett.* **89**, 186802 (2002).
53. C.R. Kagan, C.B. Murray, M. Nirmal, M.G. Bawendi, *Phys. Rev. Lett.* **76**, 1517 (1996).
54. M. Achermann, M.A. Petruska, S.A. Crooker, V.I. Klimov, *J. Phys. Chem. B* **107**, 13782 (2003).
55. S.A. Crooker, T. Barrick, J.A. Hollingsworth, V.I. Klimov, *Appl. Phys. Lett.* **82**, 2793 (2003).
56. B.N. Pal, Y. Ghosh, S. Brovelli, R. Laacharoensuk, V.I. Klimov, J.A. Hollingsworth, H. Htoon, *Nano Lett.* **12**, 331 (2011).
57. C. Galland, Y. Ghosh, A. Steinbrück, J.A. Hollingsworth, H. Htoon, V.I. Klimov, *Nat. Commun.* **3**, 908 (2012).
58. C. Galland, Y. Ghosh, A. Steinbrück, M. Sykora, J.A. Hollingsworth, V.I. Klimov, H. Htoon, *Nature* **479**, 203 (2011).
59. P.L. Redmond, L.E. Brus, *J. Phys. Chem. C* **111**, 14849 (2007).
60. L.A. Padilha, I. Robel, D.C. Lee, P. Nagpal, J.M. Pietryga, V.I. Klimov, *ACS Nano* **5**, 5045 (2011).
61. J.A. McGuire, M. Sykora, I. Robel, L.A. Padilha, J. Joo, J.M. Pietryga, V.I. Klimov, *ACS Nano* **4**, 6087 (2010).
62. V. Fomenko, D.J. Nesbitt, *Nano Lett.* **8**, 287 (2007).
63. S. Hohng, T. Ha, *J. Am. Chem. Soc.* **126**, 1324 (2004).
64. S. Jin, N. Song, T. Lian, *ACS Nano* **4**, 1545 (2010).
65. J.M. Pietryga, K.K. Zhuravlev, M. Whitehead, V.I. Klimov, R.D. Schaller, *Phys. Rev. Lett.* **101**, 217401 (2008).
66. V.I. Klimov, A.A. Mikhailovsky, D.W. McBranch, C.A. Leatherdale, M.G. Bawendi, *Science* **287**, 1011 (2000).
67. I. Robel, R. Gresback, U. Kortshagen, R.D. Schaller, V.I. Klimov, *Phys. Rev. Lett.* **102**, 177404 (2009).
68. W.K. Bae, L.A. Padilha, Y.-S. Park, H. McDaniel, I. Robel, J.M. Pietryga, V.I. Klimov, *ACS Nano* **7**, 3411 (2013).
69. T.A. Baker, J.L. Rouge, D.J. Nesbitt, *Mol. Phys.* **107**, 1867 (2009).
70. Y. Chen, J. Vela, H. Htoon, J.L. Casson, D.J. Werder, D.A. Bussian, V.I. Klimov, J.A. Hollingsworth, *J. Am. Chem. Soc.* **130**, 5026 (2008).
71. G.E. Cragg, A.L. Efros, *Nano Lett.* **10**, 313 (2009).
72. F. García-Santamaría, S. Brovelli, R. Viswanatha, J.A. Hollingsworth, H. Htoon, S.A. Crooker, V.I. Klimov, *Nano Lett.* **11**, 687 (2011).
73. F. García-Santamaría, Y. Chen, J. Vela, R.D. Schaller, J.A. Hollingsworth, V.I. Klimov, *Nano Lett.* **9**, 3482 (2009).
74. P.P. Jha, P. Guyot-Sionnest, *ACS Nano* **3**, 1011 (2009).
75. B. Mahler, P. Spinicelli, S. Buil, X. Quelin, J.-P. Hermier, B. Dubertret, *Nat. Mater.* **7**, 659 (2008).
76. Y.-S. Park, A.V. Malko, J. Vela, Y. Chen, Y. Ghosh, F. García-Santamaría, J.A. Hollingsworth, V.I. Klimov, H. Htoon, *Phys. Rev. Lett.* **106**, 187401 (2011).
77. W. Qin, P. Guyot-Sionnest, *ACS Nano* **6**, 9125 (2012).
78. X. Wang, X. Ren, K. Kahen, M.A. Hahn, M. Rajeswaran, S. Maccagnano-Zacher, J. Silcox, G.E. Cragg, A.L. Efros, T.D. Krauss, *Nature* **459**, 686 (2009).
79. M. Zavelani-Rossi, M.G. Lupo, F. Tassone, L. Manna, G. Lanzani, *Nano Lett.* **10**, 3142 (2010).
80. P. Frantsuzov, M. Kuno, B. Janko, R.A. Marcus, *Nat. Phys.* **4**, 519 (2008).
81. W.K. Bae, Y.-S. Park, J. Lim, D. Lee, L.A. Padilha, H. McDaniel, I. Robel, C. Lee, J.M. Pietryga, V.I. Klimov, *Arxiv* **1307**, 0760944 (2013).
82. C. Javaux, B. Mahler, B. Dubertret, A. Shabae, A.V. Rodina, A.L. Efros, D.R. Yakovlev, F. Liu, M. Bayer, G. Camps, L. Biadala, S. Buil, X. Quelin, J.P. Hermier, *Nat. Nanotechnol.* **8**, 206 (2013).
83. J.A. McGuire, M. Sykora, J. Joo, J.M. Pietryga, V.I. Klimov, *Nano Lett.* **10**, 2049 (2010).
84. J.A. McGuire, J. Joo, J.M. Pietryga, R.D. Schaller, V.I. Klimov, *Acc. Chem. Res.* **41**, 1810 (2008).
85. W. Koh, A.Y. Kopysov, J.T. Stewart, B.N. Pal, I. Robel, J.M. Pietryga, V.I. Klimov, *Sci. Rep.* (2013), doi 10.1038/srep02004.
86. L.A. Padilha, W.K. Bae, V.I. Klimov, J.M. Pietryga, R.D. Schaller, *Nano Lett.* **13**, 925 (2013).
87. J.I. Climente, J.L. Movilla, J. Planelles, *Small* **8**, 754 (2012).
88. Y.-S. Park, W.K. Bae, L.A. Padilha, J.M. Pietryga, V.I. Klimov, *Arxiv* **1307**, 0760938 (2013).
89. J.J. Li, Y.A. Wang, W. Guo, J.C. Keay, T.D. Mishima, M.B. Johnson, X. Peng, *J. Am. Chem. Soc.* **125**, 12567 (2003).
90. Y. Shirasaki, G.J. Supran, W.A. Tisdale, V. Bulović, *Phys. Rev. Lett.* **110**, 217403 (2013).
91. R. Osovsky, D. Cheskis, V. Kloper, A. Sashchiuk, M. Kroner, E. Lifshitz, *Phys. Rev. Lett.* **102**, 197401 (2009).
92. S. Coe, W.-K. Woo, M. Bawendi, V. Bulović, *Nature* **420**, 800 (2002).
93. A.H. Mueller, M.A. Petruska, M. Achermann, D.J. Werder, E.A. Akhador, D.D. Koleske, M.A. Hoffbauer, V.I. Klimov, *Nano Lett.* **5**, 1039 (2005).
94. J.-M. Caruge, J.E. Halpert, V. Bulović, M.G. Bawendi, *Nano Lett.* **6**, 2991 (2006). □

Custom Designed Systems for Sub-Kelvin SPM

Trusted by Today's Leading Researchers to
Explore Tomorrow's Most Advanced Materials

Dilution Refrigerators & Helium-3 Cryostats for Sub-Kelvin Scanning Probe Microscopy (SPM)



- Temperatures Range: 0.009 K - 1 K
- Fully Bakeable Systems
- Solenoid Magnets up to 17 T
- Vector Magnets up to 9-4 T or 9-1-1T
- UHV Compatible: $<10^{-10}$ Torr
- Low Helium Consumption
- Low Vibration / Low RF Noise for Atomic Resolution
- High B/T Capabilities (10^3 T/K)
- Fully Automated Gas Handling System with Color Touch-Screen provides One-Button Cool-Down

Learn more at
www.janis.com/UHV-ULT-SPM.aspx



MRS OnDemand®

*Climbing the Ladder of Density
Functional Approximations*

Watch 2012 MRS Materials Theory Award Winner,
John P. Perdew, Tulane University,
give his talk **FREE** via MRS OnDemand.

www.mrs.org/f12-mta-video